Available online at www.sciencedirect.com
ScienceDirect
Journal of Power Sources 167 (2007) 162–170
JOURNAL OF POWER SOURCES
www.elsevier.com/locate/jpowsour

Electrode structure analysis and surface characterization for lithium-ion cells simulated low-Earth-orbit satellite operation I. Electrochemical behavior and structure analysis

Xianming Wang [a,*], Yoko Sakiyama [b], Yoshikazu Takahashi [b], Chisa Yamada [a], Hitoshi Naito [a], Go Segami [a], Toshiya Hironaka [b], Eiji Hayashi [b], Kouichi Kibe [a]

[a] *Institute of Space Technology and Aeronautics, Japan Aerospace Exploration Agency, Tsukuba Space Center, Sengen 2-1-1, Ibaraki 305-8505, Japan*
[b] *Toray Research Center, Inc., Sonoyama 3-3-7, Otsu, Shiga 520-8567, Japan*

Received 15 October 2006; received in revised form 8 February 2007; accepted 8 February 2007
Available online 17 February 2007

Abstract

Lithium-ion cells for satellite applications operate under a special condition, and are expected to behave differently from those for commercial purposes. To understand the performance-degradation mechanism of lithium-ion cells experienced cycle-life testing in a simulated low-Earth-orbit (LEO) satellite operation, we conducted the structure analysis and surface characterization of the aged $LiCoO_2$ cathode and graphite anode obtained from a lithium-ion cell with 4350-cycle LEO simulation experience. The analysis results were compared with a fresh cell which served as control. This paper provides a review of testing results on electrochemical and structure analysis. The capacity-verification and impedance measure results indicated that the $LiCoO_2$ cathode, rather than graphite anode, was responsible for the performance degradation of the aged cell. This conclusion was confirmed by the structure analysis. The qualitative analysis of the XRD spectra disclosed that the aged cathode exhibited a much larger structure change than the aged anode. We also detected the lithium ions that were irreversibly reserved in graphite anode in XRD and ^7Li nuclear magnetic resonance (NMR) analysis of aged graphite anode. These results lead us to deduce that the serious structure change in $LiCoO_2$ cathode was primarily responsible for the performance degradation of the aged cell.

Keywords: Lithium-ion cell; Satellite application; Electrochemical behavior; Structure analysis; Performance-degradation mechanism

1. Introduction

So far, more than twenty spacecraft with on-board lithium-ion batteries have been reportedly launched to realize various missions [1–5]. These lithium-ion batteries offer a threefold to fourfold increase in gravimetric and volumetric energy densities and produce voltage in excess of three times the value of typical nickel-based battery systems. Due to a reduction in mass to orbit, the additional onboard capability was allowed, and the launch costs were effectively decreased. The satisfactory flight experiences confirmed the feasibility of lithium-ion batteries operated in a space environment, and encouraged more aerospace firms and organizations to pay attention to lithium-ion programs.

In the case of satellites, the rechargeable batteries are required to provide energy during orbit time spent shaded from the sun, and are about one third the weight of the satellite power system [6]. High energy density makes the lithium-ion technology an attractive choice to storage power in a satellite. Like the other battery technologies, cycle life is also a critical issue for lithium-ion batteries to determine mission duration. The overall lithium-ion program addresses much effort to assess the cycle life. However, this cycle-life demonstration is mainly limited in a real-time testing simulating low-Earth-orbit (LEO, within 1000 km from the Earth) or geosynchronous-Earth-orbit (GEO, 36,000 km from the Earth) satellite operation. There is little data on the performance-degradation mechanism of lithium-ion cells for satellite applications, though it is very important

* Corresponding author. Tel.: +81 29 868 4247; fax: +81 29 868 5969.
E-mail address: wangdai-666@mpd.biglobe.ne.jp (X. Wang).

0378-7753/$ – see front matter © 2007 Elsevier B.V. All rights reserved.
doi:10.1016/j.jpowsour.2007.02.011

to understand the cycling behavior and improve the cycling performance.

So far, we have seen in the literature more and more comprehensive reports addressing the performance degradation issue of lithium-ion cells for on-ground applications. Various surface characterization and structure analysis results of aged cell components demonstrate that the surface film at graphite anode plays an important role in cell performance degradation [7–18]. Except cycling, the temperature and prolonged storage are also the primary factors to influence cell performance. However, lithium-ion cells for satellite applications have a different operation conditions from those used on ground. Typically, a spacecraft in LEO periodically experiences about 60 min sunshine and 30 min eclipse. This requires that on-board rechargeable cells store necessary power from solar cells at a short interval of 60 min, and generate enough power to meet electrical demands of bus and mission at a very short interval of 30 min. Rechargeable cells must thus exhibit good cycling performance even at high charge and discharge rates. Additionally, the LEO satellite applications require that lithium-ion cells possess a cycle life of more than 30,000 cycles. To meet the above requirements, lithium-ion cells are operated in the moderate conditions, such as a depth of discharge (DOD) of smaller than 40% for LEO mission and an optimum temperature range from 10 to 20 °C [19,20]. These special operation conditions and requirements make it possible that lithium-ion cells for satellite applications have a different performance-degradation mechanism from those used on ground.

The primary objective of this work is to investigate the performance-degradation mechanism of commercial laminated lithium-ion cells (0.68 Ah) with $LiCoO_2$ cathode and graphite anode simulated LEO satellite operation (DOD: 40%). One aged lithium-ion cell experiencing 4350 cycle charge–discharge was taken apart and the anode and cathode were used for structure analysis (^{7}Li nuclear magnetic resonance (NMR), X-ray diffraction (XRD)) and surface characterization (Fourier transform infrared-Attenuated total reflection (FTIR-ATR), X-ray photoelectron spectroscopy (XPS)). Another fresh lithium-ion cell having the same specification was also tested as a control without cycle-life testing experience. Since the cell-performance degradation may be attributed to the electrodes rather than the electrolytes and separator in a lithium-ion cell simulated spacecraft operation in our experiences, we focused my attention on the electrode materials. In this paper, we summarize the latest results on the cycling behavior and electrode structure analysis for two types of lithium-ion cells. These data will be helpful to guide the development of future lithium-ion cell designs and chemistries for satellite applications.

2. Experimental

2.1. Sample of lithium-ion cell

The typical specifications of the laminated lithium-ion cells (0.68 Ah) evaluated in this work were described in details in our precious work [21,22]. These cells mainly consist of $LiCoO_2$ cathode, graphite anode, liquid-state organic electrolyte containing $LiPF_6$ solute and ethylene carbonate (EC) solvent, and an aluminum-laminate-film package. The aged and fresh cells were produced in the same lot. So we can attribute the difference of these two cells in electrode structure and surface phenomena to cycle-life testing experience of the aged cell.

The aged lithium-ion cell was tested by simulating satellite's LEO operation with a DOD of 40% [21]. The cycle-life testing finished after 4350 cycles.

2.2. Performance evaluation of lithium-ion cells

The aged and fresh lithium-ion cells were set on a thermostatic plate (Toyo Seisakusho, Advantec LV-600) of 19 ± 1 °C. We first conducted the capacity-verification using a charge–discharge system (Advanced Engineering Services, 2004-C101). The cells were charged in constant current–constant voltage (CC–CV) mode with a charge rate of 0.5*C*, a taper voltage of 4.1 V and a total charge time of 6 h, and discharged in CC mode with a discharge rate of 0.5*C* and a cut-off voltage of 3.0 V.

After every capacity-verification, the cell was left in the open-circuit state for at least 2 h to stabilize the cell voltage. We then measured the ac impedance with a frequency ranging from 10 kHz to 0.01 Hz at 5 mV potentiostatic signal amplitude with a Solartron FRA 1255B frequency response analyzer and a Solartron model 1287 electrochemical interface.

2.3. Destructive physical analysis

After capacity-verification testing and ac impedance measurement, the cells were destructed under a highly pure argon atmosphere in a standard glove box (Miwa). Both graphite anode and $LiCoO_2$ cathode held in full-discharge state, and were used for single-electrode-performance testing, structure analysis (NMR, XRD), and surface characterization (FTIR-ATR, XPS). The analytical samples were collected from the inner part of wounded electrode stack where the electrode subjected to relatively serious performance degradation in our knowledge. We transported the samples to instruments using airtight transfer vessels with a highly pure argon (for FTIR-ATR, XPS analysis) or nitrogen (for NMR analysis) atmosphere. We did not wash the electrode surface before used for structure analysis and surface characterization since the surface film may partly dissolve in the washing solvent in our experience.

For comparison, the same destructive physical analysis was also applied for the fresh cell.

2.4. Single-electrode-performance testing

The electrochemical performances of both electrodes were preliminarily tested in two-electrode half cells using a lithium foil (Hohsen, battery grade) counter electrode. The sandwich-type anode (cathode) half cell was assembled by contacting in sequence an anode (cathode) sheet (12.5 cm^2), a porous polypropylene separator (Celgard, battery grade), and the lithium foil, and inserted in an airtight beaker containing

1 mol dm^{-3} $LiPF_6$/EC + DEC (1:2) electrolyte. The lithium foil was enough excess in capacity ratio to the anode (cathode). All half cells were prepared under a highly pure argon atmosphere in a standard glove box (Miwa).

The single-electrode performance of the half cell was evaluated with a charge–discharge apparatus (Asuka, ACD-01) in a thermostatic program incubator (Yamato, IN600) at 20 ± 1 °C. The capacity-verification testing was conducted in the constant current–constant voltage (CC–CV) charge mode and CC discharge mode. The charge and discharge currents were set to 2.0 mA, and the cutoff voltage was set to 0.01 V and 1.5 V for the anode half cells and 4.2 V and 3.0 V for the cathode half cells. The charge duration of the CV phase was set at 7 h for both anode and cathode half cells.

After capacity-verification, the half cell was left in the open-circuit state for at least 2 h to stabilize the cell voltage. We then measured the ac impedance with the same conditions as that for the full lithium-ion cells.

2.5. XRD study

The crystal structures of graphite anodes and $LiCoO_2$ cathodes were investigated by powder X-ray diffraction (XRD) under air atmosphere. The sample was obtained by scraping the electrode sheet, and milled into powder in an agate-made mortar. Before XRD measurement, the sample powder was filled into a standard cubic frame (20 mm in width, 18 mm in length, and 0.2 mm in thickness). XRD data were collected on a diffractometer (RINT-1400, Rigaku) with graphite-monochromatized Cu Kα radiation (=0.15405 nm). The 2θ range was set from 5 to 120° in steps of 0.02°. Since the sample powder did not concern the lithium-ion diffusion during XRD measurement, we used a scan rate of 2° min^{-1}. We performed auto retrieve with Joint Committee on Powder Diffraction Standard (JCPDS) card to pick out the standard compounds corresponding to the XRD peak data.

2.6. Solid-state NMR spectroscopy

Under a high-purity argon atmosphere, the sample (graphite anode of the aged cell or fresh cell) was filled in the center of a rotor, and fixed using Teflon spacer. Then the NMR sample tube was put in an airtight container and move for NMR analysis. During the analysis, the sample atmosphere was kept under the dry nitrogen.

^{7}Li magic angle spinning (MAS) NMR experiments were carried out for graphite anodes at 116.679 MHz on a NMR spectrometer (Chemagnetics, CMX-300) with a 5.0 mm ceramic probe for MAS. A 20° pulse of 1.2 μs was used with a 1 s recycle delay. The spinning speed was 10 kHz. The spectra were taken at an ambient temperature of 20° and dry nitrogen atmosphere. All shifts were referenced to 1 mol dm^{-3} LiCl (aq.) solution at 0 ppm.

The Fourier Transform was performed to treat the NMR data with the Grams (Galactic) and Spinsight (Chemagnetics) attached in the NMR apparatus.

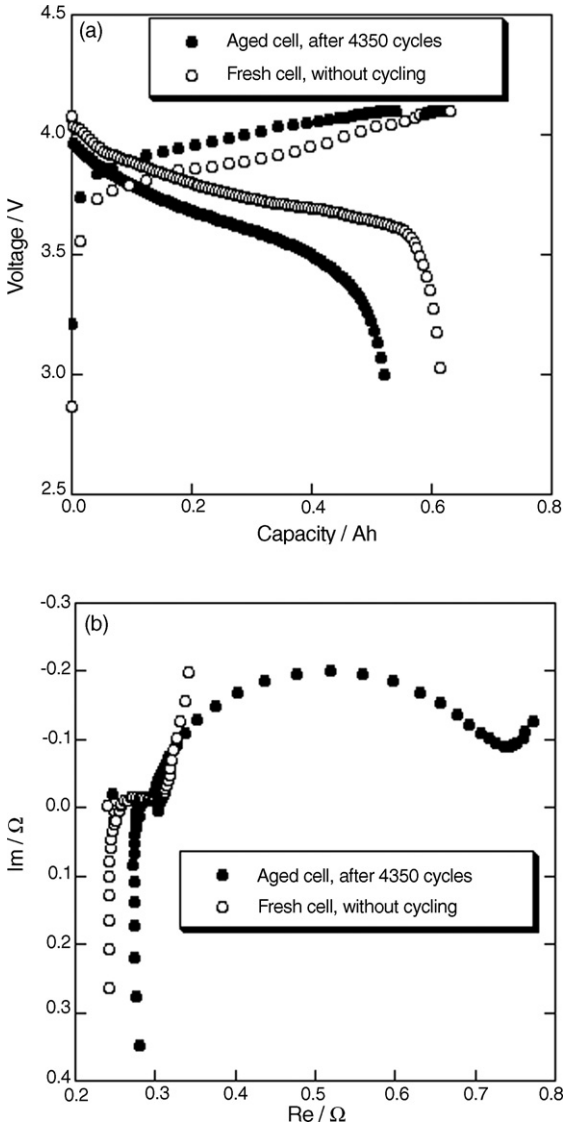

Fig. 1. (a) Capacity-verification curves and (b) Cole–Cole impedance plots for aged and fresh lithium-ion cells before used for analysis.

3. Results and discussion

3.1. Performance of lithium-ion cells

Before destructive physical analysis, we performed capacity-verification and ac impedance measurement for both aged cell and fresh cell. Fig. 1(a) shows charge–discharge curves of capacity-verification for these two cells. The discharge capacity of the aged cell was 0.54 Ah, smaller than 0.62 Ah of the fresh cell. This indicates the cell-performance degradation of the aged cell with cycling. Fig. 1(b) shows the impedance spectra of the two cells. For the aged cell, the semicircle diameter at moderate-frequency range, which mainly reflected the charge transfer resistance of cathode, played a primary role in the increase of cell internal impedance. The intercept with *X*-axis, corresponding to the connection resistance of current collector and electrolyte, and ohmic resistance of electrode, had a relatively small increase. Based on this knowledge, we focused our attention on the elec-

trode structure analysis and surface characteristics in the next step.

After destructive physical analysis, we compared the graphite anode surfaces of the aged cell and fresh cell. We observed much gold color at graphite anode surface of the aged cell as compared with that of the fresh cell. It is well known that the graphite surface shows gold color due to lithium-ion intercalation. Therefore, this observation suggests that a part of lithium ion was reserved in graphite anode with cycling. In fact, the same deduction was also conducted in our previous work [23]. In that paper, we found that the open-circuit voltage (OCV) of lithium-ion cell increased with cycling and hence deduced that a part of lithium ion was reserved in graphite anode with cycling and could not reversibly take part in the charge–discharge process again. Consequently, the graphite anode ($LiCoO_2$ cathode) active materials expanded due to lithium ion excess (lack), resulting in the detrimental cycling behavior such as electrode crumbling and excess exhaust of lithium ions due to the formation of solid electrolyte interphase (SEI) on the new electrode surface.

3.2. Single-electrode-performance testing

We performed capacity-verification and ac impedance measurement for anode and cathode of the aged cell and fresh cell by using a half cell technique in order to determine which electrode was responsible for the performance degradation of the aged cell.

Fig. 2 presents the charge–discharge curves and impedance spectra of Li/$LiCoO_2$ half cells. The $LiCoO_2$ cathode of the aged cell exhibited a steep decrease in discharge capacity and a sharp increase in impedance as compared with that of the fresh cell. This suggests that the $LiCoO_2$ cathode is responsible for the cell-performance degradation of the aged cell with cycling. We note that the aged cathode had a larger capacity fading than that of the aged lithium-ion cell. This may be explained by the different performance-degradation tendency of anode and cathode located in different areas of electrode stack. Generally, both electrodes from inner part of wounded electrode stack have relatively serious performance degradation due to less thermal dispersion and larger volume-change pressure during cycling. The analytical samples used here were just collected from the inner part of electrode stack. Additionally, the lack in electrode integrity may be another cause of relative serious capacity fading of the aged cathode, compared with that of the aged cell.

Fig. 3 depicts the charge–discharge curves and impedance spectra of Li/graphite half cells. Though the graphite anode of the aged cell had smaller discharge capacity and larger impedance than those of the fresh cell, the change degree of graphite anode in discharge capacity and impedance with cycling was much smaller than that of the $LiCoO_2$ cathode, indicating that the graphite anode was not a primary factor to affect cell-performance degradation.

In a general sense, the impedance increase due to highly-resistance film formation at electrode surface and electrode structure destruction due to volume change may be considered as the primary causes of cell-performance degradation. Next, we

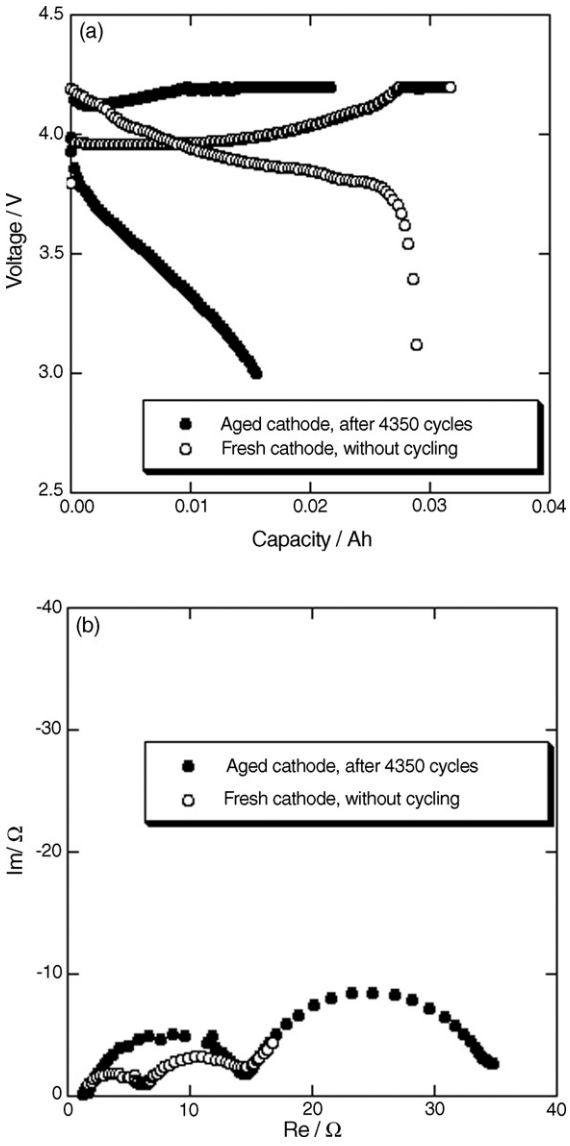

Fig. 2. (a) Capacity-verification curves and (b) Cole–Cole plots of Li/$LiCoO_2$ half cells. $LiCoO_2$ cathode materials were obtained from aged and fresh cells.

detected electrode structure change of the aged cell and fresh cell by using NMR and XRD analysis in order to find a correlation of electrode structure with cell performance.

3.3. XRD investigation

Fig. 4 compares the XRD results for cathode powders of the aged cell and fresh cell. Basically, both the aged cell and fresh cell showed the XRD profile corresponding to $Li_{1-x}CoO_2$ ($x = 0$–0.5). However, the serious peak-split phenomenon was observed for the aged cell, indicating crystalline structure change of $LiCoO_2$ with cycling.

Fig. 5 compares the XRD results for graphite anode powders of the aged cell and fresh cell. Compared with the fresh cell, the aged cell exhibited a few special phenomena. At the graphite anode of the aged cell, a trace of lithium phosphate and lithium fluoride was detected, possibly corresponding to surface-film components of the graphite anode. At low-angle

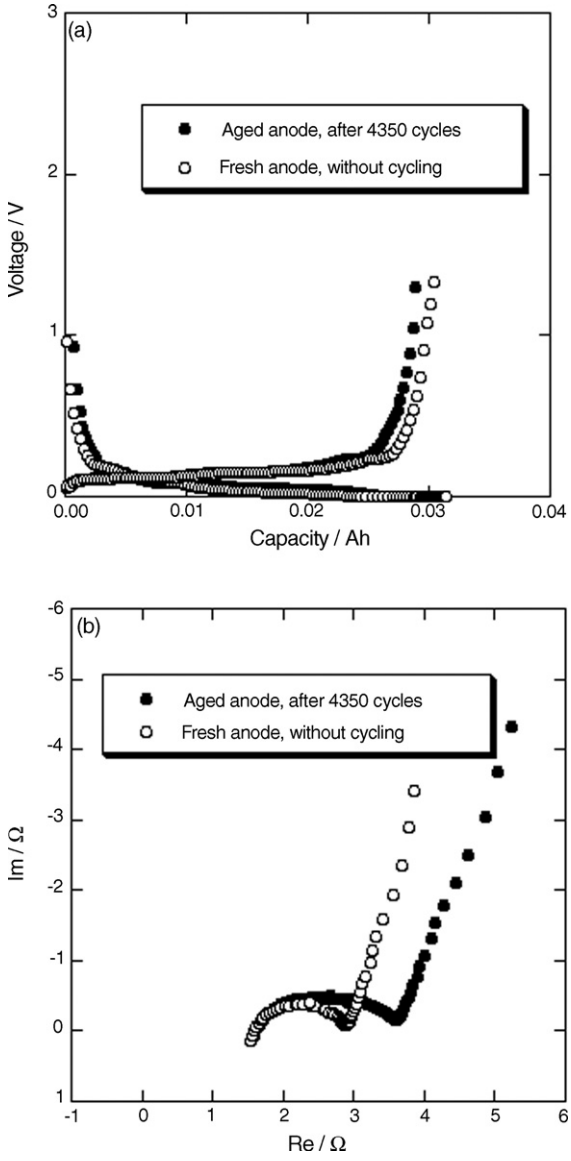

Fig. 3. (a) Capacity-verification curves and (b) Cole–Cole plots of Li/graphite half cells. Graphite anode materials were obtained from aged and fresh cells.

side, a new (0 0 2) peak was observed for the aged cell. The broad peak near $2\theta = 20^\circ$ may be assigned to glass scatter of sample holder.

Next, we performed qualitative analysis to identify the crystalline structure. We first treated the XRD chart by smoothing and background deletion. We then performed the peak searching to select the characteristic diffraction peaks with diffraction angle 2θ, interatomic spacing d, and relative peak intensity I/I_0. The crystalline size was calculated from the full width at half-maximum (FWHM) of XRD peak by using the following Scherrer formula [24].

$$L = \frac{K\lambda}{\beta_0 \cos\theta_B} \quad (1)$$

$$\beta_0^2 = \beta_E^2 - \beta_I^2 \quad (2)$$

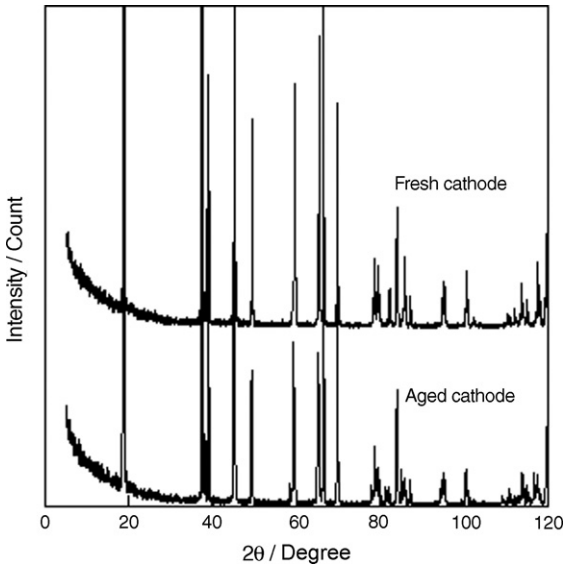

Fig. 4. Enlarged XRD pattern of $LiCoO_2$ cathodes obtained from the aged and fresh lithium-ion cells.

where L denotes crystalline size, K the constant (0.9), λ the X-ray wavelength (0.15405 nm), θ_B the Bragg angle, β_E the FWHM and β_I is the equipment constant.

Table 1 summarizes the crystalline sizes of typical peaks for the cathodes of two cells. The fresh cell exhibited the standard crystalline lattice of $LiCoO_2$. However, the aged cell exhibited some new-emerging peaks as the secondary component, except the original peaks corresponding to $LiCoO_2$ as the main component. In the above discussion, we supposed that a part of lithium ion was restricted in the graphite anode with cycling, which could not return to the cathode to take part in reversible electrode reaction again. Consequently, the lithium-ion deficiency occurred in the $LiCoO_2$ structure, resulting in lattice constant increase in c-axis direction. We believe that the new-emerging peaks correspond to the $Li_{1-x}CoO_2$ structure, where

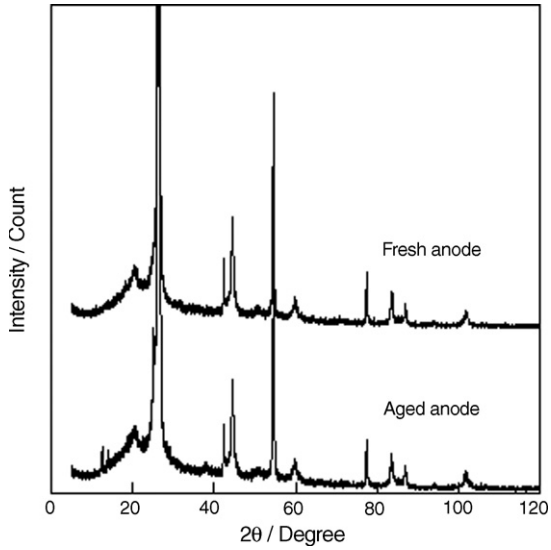

Fig. 5. Enlarged XRD pattern of graphite anodes obtained from the aged and fresh lithium-ion cells.

Table 1
Crystalline sizes of cathodes obtained from XRD pattern

Sample	*h*	*k*	*l*	2θ (°)	*d* (Å)	FWHM (°)	Crystalline size (nm)	Note
Aged cell	0	0	3	18.71	4.739	0.143	56.3	[a]
	0	0	3	18.86	4.701	0.089	90.5	
	1	0	1	37.38	2.404	0.092	91.2	
	0	0	6	37.99	2.367	0.119	70.6	
	0	0	6	38.33	2.346	0.111	75.8	[a]
	0	1	2	39.03	2.306	0.088	95.8	
	1	0	4	45.08	2.009	0.114	75.5	
	0	1	5	49.24	1.849	0.099	88.3	
	0	1	5	49.39	1.844	0.142	61.6	[a]
	0	0	9	58.47	1.577	0.126	72.3	
	0	0	9	59.05	1.563	0.099	92.2	[a]
	1	0	7	59.23	1.559	0.123	74.3	
	1	0	7	59.53	1.552	0.117	78.2	[a]
	0	1	8	64.97	1.434	0.141	66.8	
	0	1	8	65.35	1.427	0.128	73.7	[a]
	1	1	0	66.35	1.408	0.135	70.3	
	1	1	3	69.66	1.349	0.110	88.0	
Fresh cell	0	0	3	18.89	4.699	0.141	57.1	
	1	0	1	37.37	2.406	0.089	94.2	
	0	0	6	38.36	2.347	0.099	85.0	
	0	1	2	39.04	2.307	0.090	93.7	
	1	0	4	45.19	2.007	0.108	79.7	
	0	1	5	49.41	1.845	0.106	82.5	
	0	0	9	59.07	1.564	0.123	74.2	
	1	0	7	59.56	1.552	0.121	75.6	
	0	1	8	65.38	1.427	0.119	79.3	
	1	1	0	66.32	1.409	0.096	98.9	
	1	1	3	69.65	1.350	0.102	94.9	

[a] Originate from the crystalline lattice of the new-emerging peaks, which were defined as secondary component.

x reflects the lithium-ion deficiency with cycling. Additionally, we found that the crystalline size corresponding to the main component, $LiCoO_2$, for the aged cell became smaller than that for the fresh cell, indicating the crystalline destruction of cathode active material with cycling. The structure destruction of $LiCoO_2$ may be one of the factors causing cell-performance degradation.

Table 2 summarizes the crystalline sizes of typical peaks for the anodes of two cells. Compared with the cathode, the anode showed the small difference in crystalline structure after prolonged cycling. However, we found a new (0 0 2) peak for the aged cell. As indicated above, a part of lithium ion may be restricted in the anode after discharging and cannot take part in the reversible charge–discharge behavior again. We reasonably assign the new (0 0 2) peak to the carbon where irreversible lithium ions are intercalated. The crystalline size corresponding to graphite for the aged cell was also smaller than that for the fresh cell, suggesting that the cycling behavior was also harmful for graphite crystalline structure. In Table 2, a few peaks due to graphite structure were also observed, including 54° in 2θ.

Table 2
Crystalline sizes of anodes obtained from XRD pattern

Sample	*h*	*k*	*l*	2θ (°)	*d* (Å)	Half-height width (°)	Crystalline size (nm)	Note
Aged cell	0	0	2	25.18	3.537	0.659	12.4	[a]
	0	0	2	26.49	3.365	0.237	34.4	
	1	0	0	42.31	2.136	0.190	44.8	
	1	0	1	44.52	2.035	0.569	15.1	
	0	0	4	54.58	1.681	0.258	34.6	
	1	0	3	60.01	1.542	1.240	7.4	
Fresh cell	0	0	2	26.48	3.363	0.190	43.0	
	1	0	0	42.30	2.135	0.158	53.9	
	1	0	1	44.52	2.034	0.530	16.2	
	1	0	2	50.70	1.799	1.970	4.5	
	0	0	4	54.59	1.680	0.217	41.2	
	1	0	3	59.91	1.543	1.313	7.0	

[a] Peak corresponding to carbon intercalated with lithium ion.

Table 3
Lattice constants of electrode materials obtained from XRD pattern

Sample	Crystalline phase	Lattice constant (Å)	Note
$LiCoO_2$ cathode			
Aged cell	Hexagonal	$a = 2.8141$, $c = 14.189$	Secondary component with a arger c-axis constant than that of fresh cell
	Hexagonal	$a = 2.8153$, $c = 14.070$	Main component with the same c-axis constant as that of fresh cell
Fresh cell	Hexagonal	$a = 2.8164$, $c = 14.0632$	
Graphite anode			
Aged cell	Hexagonal	$a = 2.462$, $c = 6.721$	
	Hexagonal	$c = 7.07$[a]	Carbon intercalated by lithium ion. A larger c-axis constant than that of fresh cell
Fresh cell	Hexagonal	$a = 2.4634$, $c = 6.719$	

[a] Calculated from peak-separate results.

The lattice constants of cathode and anode for two cells are summarized in Table 3. Overall, the lattices concerning in the anode and cathode has the same hexagonal structure. For the aged cell, the secondary component of cathode sample and the carbon intercalated by lithium ion had larger c-axis constants than those corresponding $LiCoO_2$ and graphite lattice constants for the fresh cell. Additionally, the phase with $c = 7.07$ A for the aged anode may be assigned to the second stage compound (LiC_{12}) originated from the residual lithium ion [25]. These results agreed well with our deduction mentioned above that a part of lithium ion were restricted in the carbon anode structure, causing c-axis constant increase of both cathode and anode. To a certain extent, this confirms the accuracy of our deduction.

3.4. NMR analysis

We performed ^{7}Li magic angle spinning (MAS) NMR analysis of anode materials for the aged cell and fresh cell to investigate the lithium state in graphite anode.

Fig. 6 compares the NMR spectra of graphite anodes for the aged cell and fresh cell. The peak separation results are summarized in Table 4.

For the graphite anode of aged cell (Fig. 6(a)), a peak was observed at 0 ppm, characterizing the existence of ionic lithium compound in the carbon structure. Since this peak shows sharp spectrum, the corresponding ionic lithium compound may have lower anisotropic property. In XRD study, we detected lithium ion in the carbon structure of graphite anode for the aged cell. Here we reasonably believe that the lithium-ion compound is the restricted lithium ion which cannot be reversibly deintercalated from the graphite anode in the discharge pro-

Table 4
Peak separation of NMR data for graphite anodes

Sample	Chemical shift	Lithium-ion state
Aged cell	0 ppm	Restricted lithium ion
	−10 ppm	Lithium salt
Fresh cell	From 0 to −51 ppm	Dilute

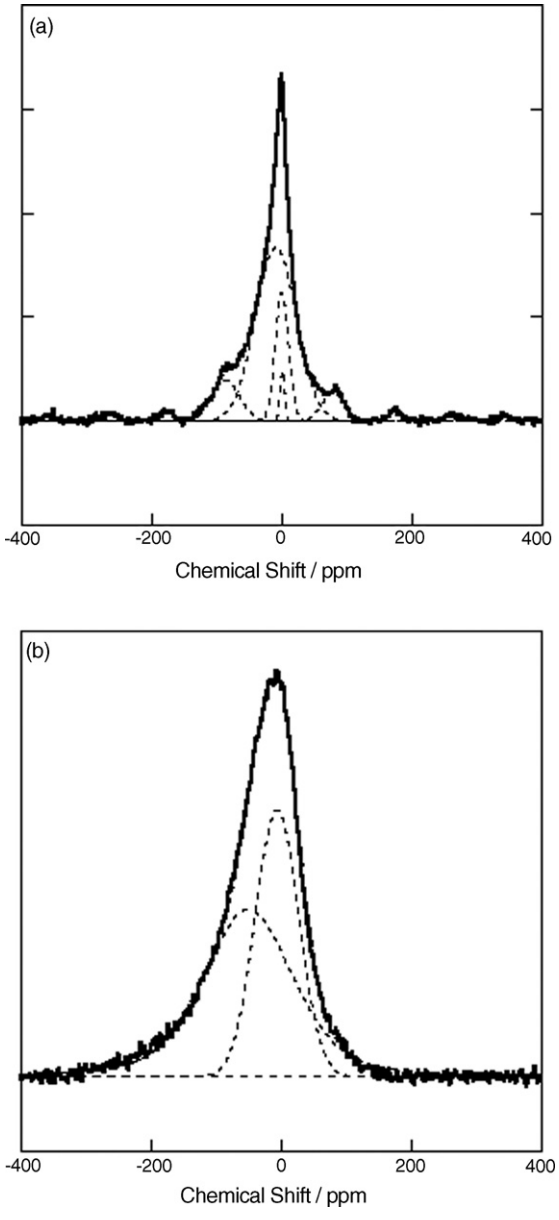

Fig. 6. Peak separation of NMR spectra for (a) aged cell graphite anode and (b) fresh cell graphite anode.

cess. Another peak was also observed near −10 ppm. Since this peak was accompanied with the other peaks as the spinning side band, we can suppose that the peak at −10 ppm corresponds to a large anisotropic lithium salt. One possible explanation is that the lithium salt at graphite surface is responsible for the peak at −10 ppm. No peak corresponding to lithium metal was observed at 260 ppm in the graphite anode of aged cell.

The graphite anode of fresh cell exhibited an asymmetrical broad peak from 0 to −50 ppm (Fig. 6(b)). Though it is difficult to assign the lithium compounds from this board peak, we are convinced that no peak exists near 0 ppm or −10 ppm, as observed in Fig. 6(a). This suggests that lithium state in the graphite anodes of two cells is different, and the observed restricted lithium ion and the lithium salt at the graphite anode for the aged cell originate from the cell-performance degradation with cycling. The peak separation indicates that the broad peak may be composed of a few large anisotropic lithium compounds. In fact, the fresh cell had a low OCV of 3.11 V before destructive physical analysis. This suggests that there is very little lithium ion in the graphite anode of fresh cell, and the lithium ion at the carbon structure is in a "dilute" state, a phase before stage structure formation [26]. We believe that the broad peak from 0 to −50 ppm may be attributed to the "dilute" lithium ion.

The capacity-testing results suggest that cathode was responsible for the cycling-performance degradation of the aged lithium-ion cell. Furthermore, we detected the partial lithium consumption at the anode and the impedance buildup at the cathode during cycling for the aged cell. We believe that these performance-degradation factors were caused by the structure change of cathode based on the XRD data. For a commercial lithium-ion cell with a cycling life of about 500, the cathode structure change may not be a primary degradation factor. However, the aged cell used in this work experienced continuous 4350 cycles in a simulated LEO satellite operation. In another paper, we reported that serious volume change in the aged cell was an irreversible degradation process. Therefore, the phase change of cathode during changing was important especially for a cell simulated a LEO operation.

4. Conclusions

We investigated the performance-degradation mechanism of an aged commercial laminated lithium-ion cell with $LiCoO_2$ cathode and graphite anode experienced 4350 cycle charge–discharge in a simulated LEO satellite operation. We took the cell apart, and conducted the capacity-verification and structure analysis of single electrode. The analysis results were compared with a fresh cell which served as controls in order to extract the cycling effect on cell performance.

Capacity-verification and impedance measure results indicated that the $LiCoO_2$ cathode, rather than graphite anode, was responsible for the performance degradation of the aged cell. This result was confirmed by the structure analysis of both $LiCoO_2$ cathode and graphite anode obtained from the aged cell in full-discharge state. XRD analysis disclosed that the aged cathode exhibited a much larger structure change than the aged anode. A new component with a large lattice constant in *c*-axis was found in XRD spectra of the aged cathode. NMR and XRD analysis of graphite anode detected the lithium ions that were irreversibly reserved inside graphite layer.

We deduced that a part of lithium ion was reserved in graphite anode with cycling and could not reversibly take part in the charge–discharge process again. Consequently, the lithium ion deficiency (excess) occurred in the $LiCoO_2$ (graphite) structure, resulting in lattice constant increase in *c*-axis direction. We believe that this structure change in $LiCoO_2$ cathode is primary causes of cell-performance degradation during long-term cycle-life testing.

Acknowledgment

The authors would like to acknowledge the technical staffs from Ryoei Technica Corporation for their support.

References

[1] R. Bugga, M. Smart, L. Whitcanack, J. Knight, R. Ewell, R. Surampudi, Proceedings of the 2002 NASA Aerospace Battery Workshop (CD-ROM Version), Marshall Space Flight Center, Huntsville, USA, 2003.
[2] A. Bennetti, R. Spurrett, C. Thwaite, N. Russel, Proceedings of the 7th European Space Power Conference (CD-ROM Version), Stresa, Italy, 2005.
[3] R. Gitzendanner, E. Jones, C. Deroy, D. Carmen, Proceedings of the 7th European Space Power Conference (CD-ROM Version), Stresa, Italy, 2005.
[4] J. Semerie, G. Dudley, J. Hausser, Proceedings of the 7th European Space Power Conference (CD-ROM Version), Stresa, Italy, 2005.
[5] T. Kiyokawa, H. Yamazaki, M. Goto, T. Gonai, Proceedings of the 2002 NASA Aerospace Battery Workshop (CD-ROM Version), Marshall Space Flight Center, Huntsville, USA, 2003.
[6] J.K. McDermott, in: J.R. Wertz, W.J. Larson (Eds.), Space Mission Analysis and Design, third ed., The Space Technology Library, California, 1999, p. 407.
[7] R. Dedryvere, S. Laruelle, S. Grugeon, L. Gireaud, J.-M. Tarascon, D. Gonbeau, J. Electrochem. Soc. 152 (2005) A689.
[8] E. Peled, J. Electrochem. Soc. 126 (1979) 2047.
[9] E. Peled, in: J.-P. Gabano (Ed.), Lithium Batteries, Academic Press, New York, 1983, p. 43.
[10] G. Nazri, R.H. Muller, J. Electrochem. Soc. 132 (1985) 2050.
[11] D. Aurbach, A. Zaban, J. Electrochem. Soc. 142 (1995) 7.
[12] D. Aurbach, Y. Cohen, J. Electrochem. Soc. 143 (1996) 3525.
[13] D. Aurbach, Y. Cohen, J. Electrochem. Soc. 144 (1997) 3355.
[14] H. Ota, Y. Sakata, X. Wang, J. Sasahara, E. Yasukawa, J. Electrochem. Soc. 151 (2004) A437.
[15] R. Spotnitz, J. Power Sources 113 (2003) 72.
[16] M. Wohlfahrt-Mehrens, C. Vogler, J. Garche, J. Power Sources 127 (2004) 58.
[17] M. Broussely, S. Herreyre, P. Biensan, P. Kasztejna, K. Nechev, R.J. Staniewicz, J. Power Sources 97 (2001) 13.
[18] R. Yazami, Electrochim. Acta 45 (1999) 87.
[19] Y. Sone, X. Wang, H. Kusawake, S. Kuwajima, Proceedings of the 2002 NASA Aerospace Battery Workshop (CD-ROM Version), Marshall Space Flight Center, Huntsville, USA, 2003.
[20] X. Wang, H. Naito, C. Yamada, G. Segami, K. Kibe, Proceedings of the 3rd International Energy Conversion Engineering Conference (CD-ROM Version), San Francisco, USA, 2005.
[21] X. Wang, C. Yamada, H. Naito, S. Kuwajima, J. Power Sources 140 (2005) 129.

[22] X. Wang, M. Kato, C. Yamada, H. Naito, G. Segami, S. Kuwajima, J. Electrochem. Soc. 153 (2006) A89.
[23] X. Wang, Y. Sone, S. Kuwajima, J. Electrochem. Soc. 151 (2004) A273.
[24] V.A. Drits, D.D. Eberl, J. Írodoñ, Clays Clay Miner. 45 (1997) 461.
[25] T. Ohzuku, Y. Iwakoshi, K. Sawai, J. Electrochem. Soc. 140 (1993) 2490.
[26] J.R. Dahn, A.K. Sleigh, H. Shi, B.M. Way, W.J. Weydanz, J.N. Reimers, Q. Zhong, U. von Sacken, in: G. Pistoia (Ed.), Lithium Batteries: New Materials, Developments, and Perspectives, Elsevier, Amsterdam, 1994.